Solution Structure of the Variable-Type Domain of the Receptor for Advanced Glycation End Products: New Insight into AGE−RAGE Interaction[†,‡]

Shigeyuki Matsumoto,[§] Takuya Yoshida,[§] Hiroko Murata,[§] Shusaku Harada,[§] Naoko Fujita,[#] Shota Nakamura,[§,||] Yasuhiko Yamamoto,[⊥] Takuo Watanabe,[⊥] Hideto Yonekura,[@] Hiroshi Yamamoto,[⊥] Tadayasu Ohkubo,*[,§] and Yuji Kobayashi*[,#]

Graduate School of Pharmaceutical Sciences, Osaka University, 1-6 Yamadaoka, Suita, Osaka 565-0871, Japan, Graduate School of Medical Sciences, Kanazawa University, 13-1 Takara-machi, Kanazawa, Ishikawa 920-8640, Japan, Department of Biochemistry, Kanazawa Medical University, 1-1 Daigaku, Uchida, Kahoku-gun, Ishikawa 920-0293, Japan, and Osaka University of Pharmaceutical Sciences, 4-20-1 Nasahara, Takatsuki, Osaka 569-1094, Japan

Received May 15, 2008; Revised Manuscript Received September 23, 2008

ABSTRACT: Diabetes is defined by chronic hyperglycemia due to deficiency in insulin action. It has been found that the amount of advanced glycation end products (AGE) from the Maillard reaction between proteins and sugar molecules increases in blood of diabetic patients and furthermore that AGE binding to their cell surface receptor (RAGE) triggers both macrovascular and microvascular impairments to cause diabetic complications. Due to the clinical significance of the vascular complications, RAGE is currently a focus as an attractive target for drug discovery of candidates which interfere with AGE−RAGE binding to prevent the subsequent intracellular signaling related to pathogenical effects. Here, we determined the three-dimensional structure of the recombinant AGE-binding domain by using multidimensional heteronuclear NMR spectroscopy and showed that the domain assumes a structure similar to those of other immunoglobulin V-type domains. The site-directed mutagenesis studies identified the basic amino acids which play a key role in the AGE binding activities. Our results obtained from this study provide new insight into AGE−RAGE interaction.

The number of diabetic patients is dramatically increasing around the world. Diabetic conditions induce several pathologic disorders. In particular, they result in both macrovascular and microvascular impairments which in turn lead to various diabetic complications such as atherosclerosis, retinopathy, and nephropathy (*1*). It is now widely accepted that prevention of diabetic vascular complications is crucial to extending human life spans and to improving the quality of life of diabetic patients.

Advanced glycation end product (AGE)[1] is a generic term for products resulting from complex Maillard reactions between proteins and reducing sugars or aldehydes, which include dehydration, condensation, cross-linking, and other reactions (*2, 3*). It has been shown that these reactions which proceed in vitro occur in blood and tissues as well (*4*). Furthermore, it is noteworthy that AGE formation is especially accelerated under the diabetic conditions defined by chronic hyperglycemia. While AGE themselves have not been well characterized so far because of their diversity, AGE cause dysfunction of vascular wall components not only by direct modifications of tissue proteins but also via interactions with their cell surface receptor [receptor for AGE (RAGE)] (*2, 5*−*9*), by disordering the growth and function of vascular cells.

Current studies have revealed that the AGE−RAGE interaction triggers the intracellular signaling which activates the proinflammatory transcriptional factor NF-κB as one of the most consistent cellular responses to this interaction (*10, 11*). The activation upregulates RAGE gene expression itself because the promoter region of this gene contains the NF-κB binding sites (*5, 12*). In the lesions of diabetic patients, AGE accumulate, thus increasing the level of expression of RAGE. These events accelerate vascular cell disturbances which result in the development of macro- and microangiopathies (*7, 13*). Such an involvement of RAGE was demonstrated

[†] This work was supported by a Grant-in-Aid for High Technology Research from the Ministry of Education, Science, Sports and Culture of Japan.

[‡] The atomic coordinates (PDB entry 2E5E for the solution structure of vRAGE) have been deposited in the Protein Data Bank, Research Collaboratory for Structural Bioinformatics, Rutgers University, New Brunswick, NJ.

* To whom correspondence should be addressed. Y.K.: Osaka University of Pharmaceutical Sciences, 4-20-1 Nasahara, Takatsuki, Osaka 560-1094, Japan; telephone, +81-72-690-1080; fax, +81-72-690-1081; e-mail, kobayasi@gly.oups.ac.jp. T.O.: Graduate School of Pharmaceutical Sciences, Osaka University, 1-6 Yamadaoka, Suita, Osaka 565-0871, Japan; telephone, +81-6-6879-8223; fax, +81-6-6879-8221; e-mail, ohkubo@phs.osaka-u.ac.jp.

[§] Osaka University.

[||] Present address: Research Institute for Microbial Diseases, Osaka University, Osaka 565-0871, Japan.

[⊥] Kanazawa University.

[@] Kanazawa Medical University.

[#] Osaka University of Pharmaceutical Sciences.

[1] Abbreviations: AGE, advanced glycation end product(s); esRAGE, endogenous secretory RAGE; BSA, bovine serum albumin; SDS−PAGE, sodium dodecyl sulfate−polyacrylamide gel electrophoresis; NMR, nuclear magnetic resonance; HSQC, heteronuclear single-quantum coherence spectroscopy; COSY, correlated spectroscopy; TOCSY, total correlation spectroscopy; NOE, nuclear Overhauser effect; NOESY, nuclear Overhauser enhancement spectroscopy; HRP, horseradish peroxidase; SPR, surface plasmon resonance; rmsd, root-mean-square deviation.

10.1021/bi800910v CCC: $40.75
Published on Web 10/29/2008

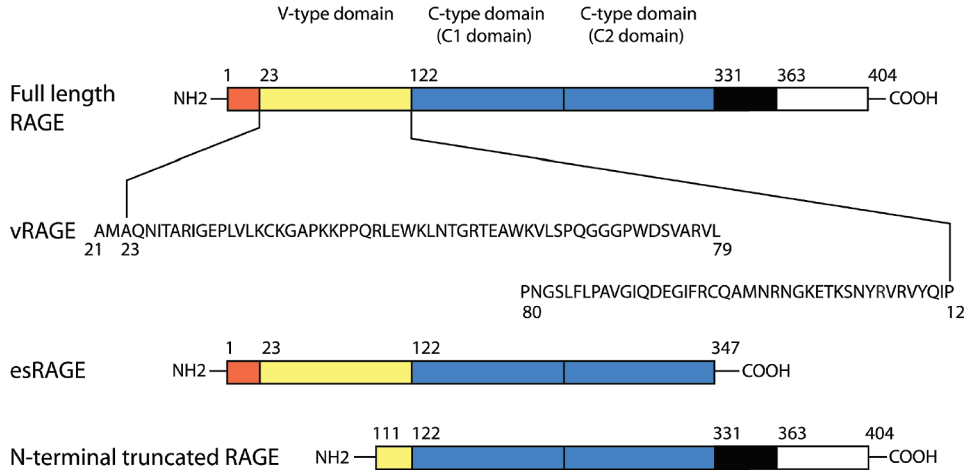

FIGURE 1: Schematic diagrams of domain structures of full-length RAGE and the splicing variants. RAGE domain structures and diagrams of splicing variants of RAGE are schematically depicted. Full-length RAGE, esRAGE, and N-terminally truncated RAGE are shown at the top, middle, and bottom, respectively. The signal peptide region, variable-type domain, constant-type domain, transmembrane-spanning region, and cytoplasmic domain are represented by boxes colored red, yellow, blue, black, and white, respectively. The primary structure of vRAGE used in this study is shown in one-letter code. In the primary structure of vRAGE, one alanine and one methionine, which are not found in that of wild-type RAGE, were appended to the N-terminus due to the primer design.

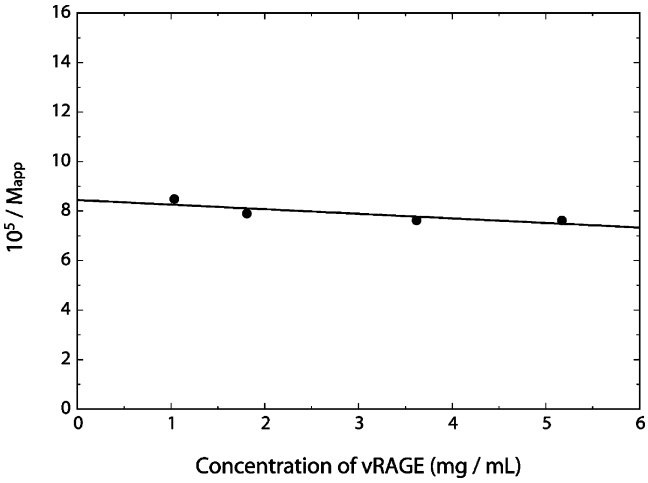

FIGURE 2: Relationship between the protein concentration and observed molecular weight (M_{app}). The mean molecular weight (M_w), which corresponds to the reciprocal of the intercept on the ordinate at zero concentration, was calculated to be 1.18×10^4, which suggests that vRAGE exists as a monomer under the given condition.

experimentally by the fact that transgenetic RAGE-overexpressing diabetic mice showed the exacerbation of diabetic vascular complication of the kidney, but RAGE-knocked out ones showed marked improvement (*8, 9*).

Judging from its amino acid sequence, RAGE is assumed to be a single-span transmembrane protein with a cytoplasmic domain required for signal transduction, a transmembrane-spanning region, and an extracellular region. Furthermore, the extracellular region is assumed to belong to the immunoglobulin superfamily and to consist of a variable-type domain (V-type domain) and two constant-type domains (C-type domain; C1 domain and C2 domain) (*6*) (Figure 1). The AGE binding site is shown to be located on the V-type domain of RAGE with the splicing variants of RAGE (*14*) (Figure 1). Despite extensive biological studies on RAGE, there have been two serious obstacles remaining in elucidating the AGE−RAGE interactions. One is the fact that AGE themselves have not been well characterized so far because of their heterogeneous and diverse nature. The other is that the structure of RAGE has not been determined.

From lesion sites in human tissues, several chemicals with low molecular weights were identified as AGE-related chemicals in past studies. However, none of them show enough detail about their in vivo activities. There has been no simple compound isolated as AGE from any reaction mixture of the Maillard reaction. Thus, no sample of AGE to satisfy the requirements for an investigation at the molecular level is yet available. As a result, certain reaction mixtures of proteins and reducing sugars or aldehydes which exhibit activities of in vitro and/or in vivo assays have been treated as AGE without further purification. In this experiment, we used Lys−AGE in addition to BSA−AGE which have been conventionally used. Both in vivo and in vitro activities have been shown for BSA−AGE, a reaction mixture of BSA and glyceraldehyde, but only in vitro activity has been shown for Lys−AGE, a reaction mixture of L-lysine and glyceraldehyde (*15*).

Under these circumstances, Chazin et al. recently investigated the ligand interaction on RAGE by SPR measurements (*16*). As a ligand, they used S100B, which is not an AGE but a cytokine known to cause inflammation through its binding with RAGE, and analyzed the mechanism using a virtual structure of RAGE constructed by assuming that the RAGE molecule should take an immunoglobulin fold. They argued that the V-domain and one of the C-domains (C1 domain, which follows the V-domain) behave as a structural unit.

To obtain sufficient information to understand the AGE−RAGE interaction, we have determined the three-dimensional structure of the recombinant V-type domain of human RAGE (vRAGE) by using multidimensional heteronuclear NMR spectroscopy (Figure 1). By investigating the binding of BSA−AGE and Lys−AGE to vRAGE from the resulting structure, we characterized the AGE−RAGE interaction. The binding profile was confirmed by mutagenesis studies on vRAGE.

These results provide the first insight into the mechanism of the AGE−RAGE interaction.

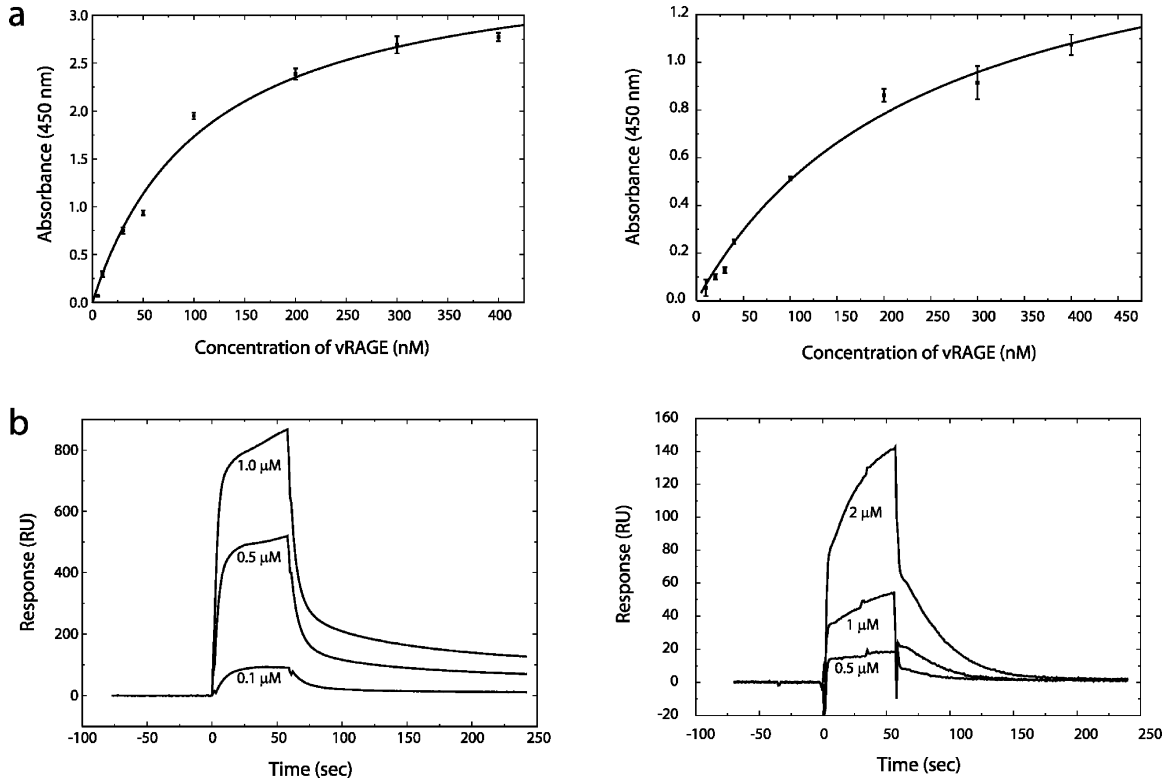

FIGURE 3: (a) Analysis of the binding of vRAGE to BSA−AGE (left) and Lys−AGE (right) using an ELISA. Vertical bars indicate means ± the standard deviation at eight different vRAGE levels ($n = 3$ each). (b) SPR analysis of vRAGE binding to BSA−AGE (left) and Lys−AGE (right). Concentrations in the figure indicate those of vRAGE at each sensorgram. All sensorgrams were corrected by subtraction of background responses.

EXPERIMENTAL PROCEDURES

Expression and Purification of vRAGE. Plasmid pCI-neo (Promega, Madison, WI) encoding esRAGE was provided by H. Yonekura et al. (*14*). A pET32b vector (Novagen), which contains the vRAGE gene (Ala23−Pro121) amplified by PCR between NcoI and XhoI restriction sites, was constructed as an expression vector designed to express the fusion protein with the thioredoxin tag, S tag, and His tag and was introduced into *Escherichia coli* strain origami B(DE3). The cells transformed by the expression vector were cultured at 37 °C to an OD_{660} of 0.6, and protein overexpression was induced by adding isopropyl 1-thio-β-D-galactopyranoside (IPTG) to a final concentration of 1 mM, followed by induction for 4 h at 37 °C. The cells were harvested by centrifugation, resuspended in buffer A [50 mM Tris-HCl (pH 8.0), 500 mM NaCl, 1 mM phenylmethanesulfonyl fluoride (PMSF), and 5% glycerol], and disrupted by sonication. The lysate was centrifuged to remove insoluble debris. The supernatant was dialyzed against buffer A for 6 h and was loaded on a HiTrap Chelating HP column (GE Healthcare) equilibrated with buffer A. The protein was eluted with a gradient of imidazole, and the eluted fraction containing vRAGE was dialyzed against buffer B [50 mM Tris-HCl (pH 8.0), 250 mM NaCl, and 10 mM $CaCl_2$]. The solutions containing vRAGE were treated with EKMax Enterokinase (Invitrogen) for 14 h at room temperature followed by inactivation of EKMax via addition of PMSF to a final concentration of 1 mM. The solutions containing vRAGE were loaded on a HiTrap Chelating HP column equilibrated with buffer A to remove the thioredoxin tag, S tag, and His tag. The fraction which was not trapped by the column was dialyzed against buffer C [20 mM sodium phosphate (pH 7.5), 250 mM NaCl, 1 mM PMSF, and 5% glycerol] and was loaded on a HiTrap Heparin HP column (GE Healthcare) equilibrated with buffer C. The protein was eluted with a gradient of NaCl. The eluted fractions containing vRAGE were analyzed by SDS−PAGE to confirm sample mass and sample purity.

Sedimentation Equilibrium. The sedimentation equilibrium experiments were performed with a Beckman-Coulter Optima XL-I analytical ultracentrifuge at a rotor speed of 36000 rpm and 25 °C with interference optics. vRAGE was dissolved in NMR measurement buffer [20 mM sodium phosphate (pH 7.5) and 100 mM Na_2SO_4] at concentrations of 1.0, 1.8, 3.6, and 5.2 mg/mL. The apparent molecular weight (M_{app}) was estimated from the following equation:

$$J(r) = J_0(r_0)\exp[(r^2 - r_0^2)(1 - \bar{v}\rho)M_{app}\omega^2/2RT]$$

where r is the radius from the center of the rotor, $J_0(r_0)$ is the displacement of fringe at a reference point, r_0, $J(r)$ is that at position r, $\bar{v}$ is the partial specific volume, ρ is the density of the solvent, ω is the angular velocity of the rotor (in radians per second), R is the universal gas constant, and T is the absolute temperature. The partial specific volume of vRAGE (0.739 cm^3/g) was estimated from the amino acid composition by the method of Cohn and Edsall (*17*).

AGE Preparation. Two kinds of AGE were prepared. One was obtained as a reaction mixture of L-lysine and glyceraldehyde and the other as a reaction mixture between albumin and glyceraldehyde. For the former, 0.09 g of L-lysine (Wako) and 0.45 g of DL-glyceraldehyde (Nacalai Tesque) were dissolved in 50 mL of 0.2 M sodium phosphate (pH 7.4) and incubated at 37 °C for 1 week shielded from light. Aliquots of the reaction mixture were named Lys−AGE and used as a ligand for RAGE. For the latter, 1.25 g of bovine

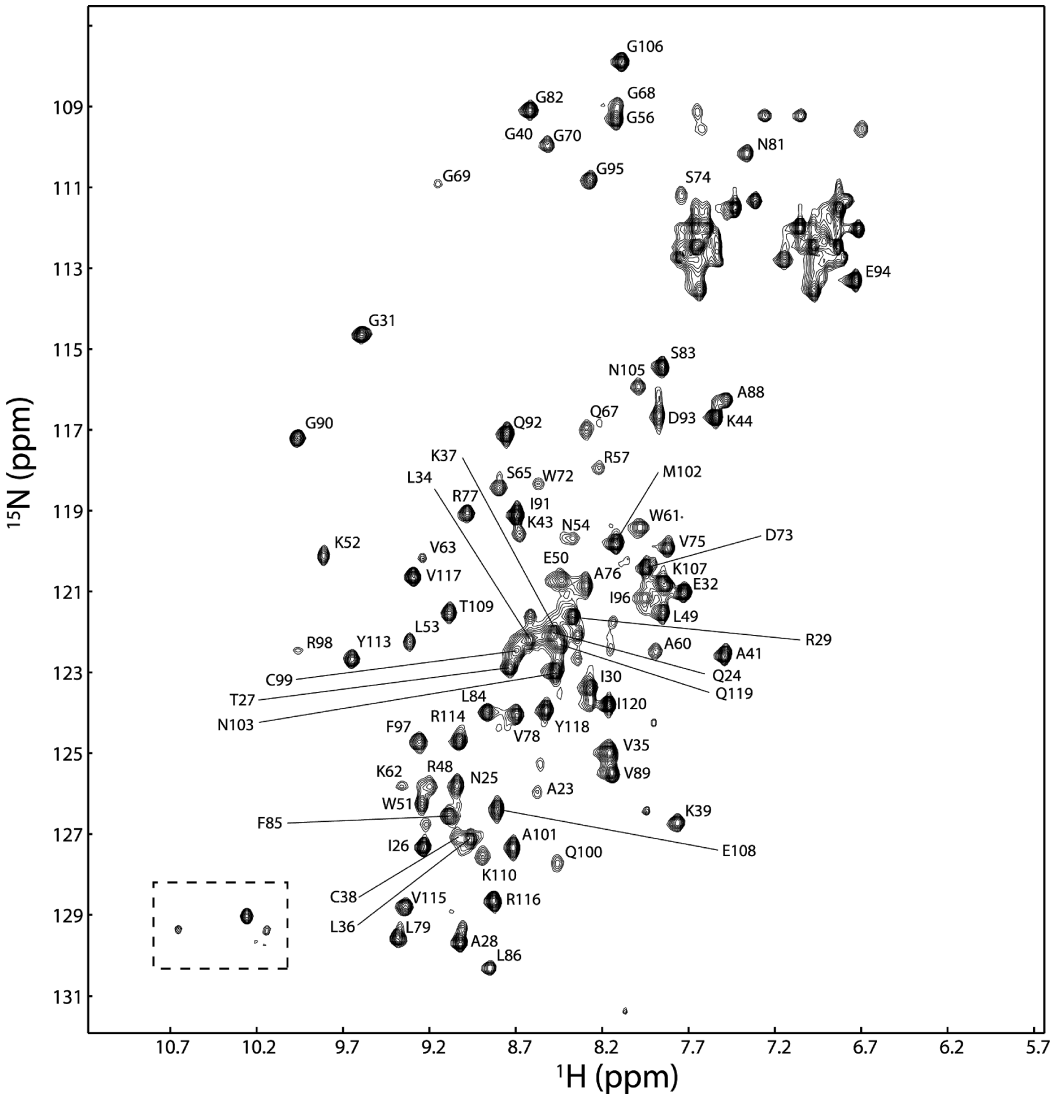

FIGURE 4: ^{1}H−^{15}N HSQC spectrum of vRAGE. The ^{1}H−^{15}N HSQC spectrum of vRAGE is shown with assignments for the cross-peaks. The cross-peaks of the Trp side chain NH groups are indicated by the dashed rectangle.

serum albumin (BSA; fatty-acid free; low endotoxin; Sigma catalog no. A8806) and 2.25 g of DL-glyceraldehydes (Nacalai Tesque) were dissolved in 50 mL of 0.2 M sodium phosphate (pH 7.4) and incubated at 37 °C for 1 week shielded from light. The reaction mixture was dialyzed against 0.2 M sodium phosphate (pH 7.4) containing 0.15 M NaCl. Aliquots of this mixture named BSA−AGE, which has been known to show pathogenic effects such as the retardation of pericyte growth and the tube formation of microvascular endothelial cells, were used as the other ligand for RAGE (*18, 19*).

Site-Directed Mutagenesis. We created mutants of vRAGE by using the QuickChange protocol (Stratagene). The Lys residues at positions 39, 43, 44, 52, 107, and 110 and the Arg residues at positions 48, 98, and 104 are substituted with Ala. The primers had the following 5′ to 3′ sequences: GGTGCTGAAGTGTGCGGGGGCCCCCAAGA,AAGGGGGC-CCCCGCGAAACCACCCCAG, GGGCCCCCAAGGCAC-CACCCCAGCG, CAGCGGCTGGAATGGGCGCTGAA-CACAGGCCGG,TGAACAGGAATGGAGCGGAGACCAAGTCCA, GGAAAGGAGACCGCGTCCAACTACCGAGTC, CCCAA-GAAACCACCCCAGGCGCTGGAATGGAAACTGAAC, C A G G A T G A G G G G A T T T T C G C G T G C C A G - GCAATGAACAGG, and CGGTGCCAGGCAATGAACGC-GAATGGAAAGGAGACCAAG, respectively. The Asn residue at position 81 is substituted with Asp. The primer had the following 5′ to 3′ sequence: CGTGTCCTTC-CCGACGGCTCCCTCTTC. The double mutant was created by using a combination of these primers. In the case of the triple mutant, the primer for the substitution of the Lys residue at position 44 had the following 5′ to 3′ sequence: GGGCCCCCGCGGCACCACCCCAGCG. The procedures for expression and purification of all mutants were almost identical to those of wild-type vRAGE. In the last step of the purification, to prevent the influence of the mutation on the affinity for heparin, a Superdex 75 column (GE Healthcare) was used instead of a HiTrap Heparin HP column.

Circular Dichroism Spectroscopy. CD spectra were recorded in 20 mM sodium phosphate (pH 7.5) and 100 mM Na_2SO_4 at 25 °C on a Jasco J-720 spectropolarimeter. Far-UV CD spectra were monitored from 200 to 250 nm using a protein concentration of 10 μM with a path length of 1 mm, a 100 mdeg sensitivity, a response time of 2 s, and a scan speed of 40 nm/min. The spectra were recorded as a four-scan averaged value.

NMR Spectroscopy. Uniformly ^{13}C- and ^{15}N-labeled vRAGE was obtained from the cells cultured in CHL medium (Chlorella Industry). The NMR samples of vRAGE

Table 1: NMR and Refinement Statistics for Protein Structures

NMR Distance and Dihedral Constraints	
no. of distance constraints	
total NOE	1032
intraresidue	455
interresidue	577
sequential ($\|i - j\| = 1$)	292
medium-range ($\|i - j\| \leq 4$)	71
long-range ($\|i - j\| \geq 5$)	219
hydrogen bonds	42
total no. of dihedral angle restraints	
ϕ	110
ψ	110
Structural Statistics	
deviations from idealized geometry	
bond lengths (Å)	0.0010 ± 0.0001
bond angles (deg)	0.285 ± 0.002
impropers (deg)	0.092 ± 0.004
average pairwise rmsd[a] (Å)	
well-defined residues[b]	
backbone	0.40
heavy	0.73
all residues	
backbone	1.17
heavy	1.54

[a] Pairwise rmsd calculated among 15 refined structures. [b] Gln24−Lys37, Leu49−Thr55, Pro71−Gln100, and Tyr113−Val117.

were prepared in NMR measurement buffer [20 mM sodium phosphate (pH 7.5) and 100 mM Na_2SO_4] prepared in 10% D_2O or 99% D_2O at a final concentration 0.4−0.6 mM. All NMR experiments were carried out at 25 °C on a Varian INOVA600 or INOVA500 instrument equipped with shielded gradient triple-resonance probes.

^{15}N heteronuclear single-quantum coherence (HSQC), HNCACB, CBCACONH, HNCA, HNCO, HNCACO, HNCAHA, and HBHACONH spectra were acquired for assignments of the backbone signals. ^{13}C ctHSQC, (H)C-(CO)NH-total correlated spectroscopy (TOCSY), H(CCO)NH-TOCSY, and CCH-TOCSY spectra were acquired for assignments of aliphatic side chain signals. ^{13}C ctHSQC and ^{13}C-separated nuclear Overhauser effect spectroscopy (NOESY) spectra of the aromatic region and (Hβ)Cβ(CγCδ)Hδ spectra were acquired for assignments of aromatic side chain signals. ^1H NOESY and ^1H TOCSY spectra were acquired for assignments of α-protons in β-sheet region and aromatic side chains. ^{15}N-separated NOESY and ^{13}C-separated NOESY spectra were acquired for collection of information about the distance between two hydrogen atoms in the protein. The $^1H-^{15}N$ steady state nuclear Overhauser effect (NOE) spectrum was acquired using HSQC-type pulse sequences. The NOE values were obtained from the ratios of cross-peak intensities derived from the spectra acquired with and without a 3.5 s saturation of amide protons. The backbone amide protons that exchanged slowly with solvent were identified by comparing the ^{15}N HSQC spectrum acquired 1 h after transfer to 99.9% D_2O buffer with the spectrum acquired in 10% D_2O buffer. NMR samples in 99.9% D_2O buffer were prepared by dissolving the lyophilisate of vRAGE. To investigate the influence of site-directed mutagenesis on the spatial structure, we conducted ^{15}N HSQC measurements on the triple mutant, K43A/K44A/R104A, and the single mutant, N81D. For experimental details of NMR spectroscopy, readers are referred to the review in ref *20*.

All NMR data were processed and analyzed with NMRPipe (*21*) and NMRView (One Moon Scientific, Inc.), and programs written in-house.

Structural Calculations. NOEs were classified as strong, medium, and weak, corresponding to distance restraints of 1.8−2.8, 1.8−3.4, and 1.8−5.0 Å, respectively. The information about backbone hydrogen bonds was obtained from the results of amide proton exchange experiments and initial structure calculations tentatively obtained only on the basis of NOE and dihedral angle restraints. For each of the hydrogen bonds, two distance restraints were adopted, 3.3 Å between the amide nitrogen atom and the carbonyl oxygen atom and 2.3 Å between the amide proton and the carbonyl oxygen atom. Hydrogen bond restraints were incorporated in the later stage of the structure calculation. By using TALOS (*22*), the dihedral angle restraints were calculated from chemical shifts of HN, N, Cα, Hα, Cβ, and C′ atoms of a triplet of the residues in the primary structure of vRAGE. In addition to these restraints, the restraints of the disulfide bond between Cys38 and Cys99 were adopted. On the basis of these restraints, the structure calculations were carried out by using CNS solve 1.1 (*23*), and further analysis of the final structures was carried out using MOLMOL (*24*), PyMOL (http://www.pymol.org), and PROCHECK-NMR (*25*).

Enzyme-Linked Immunosorbent Assay (ELISA). ELISAs were carried out at 25 °C on a BECKMAN COULTER-AD340 instrument. The BSA−AGE and Lys−AGE solutions were prepared at concentrations of 4.7 and 0.28 μg/mL, respectively, in 10 mM sodium phosphate buffer (pH 7.4) containing 0.15 M NaCl. A RAGE antibody named RAGE(N16) (Santa Cruz) and an anti-goat IgG-HRP antibody (Santa Cruz) were dissolved at a concentration of 0.5 μg/mL in buffer D [20 mM Tris-HCl (pH 7.5), 0.15 M NaCl, and 0.01% Tween 20], and the solutions were used as the primary reagents and the secondary reagents, respectively. Polystyrene 96-well microplates (Maxisorp, Nunc) were coated with 100 μL of these AGE solutions for 24 h at 4 °C. The unoccupied wells were blocked with 300 μL of blocking buffer [20 mM Tris-HCl (pH 7.5), ProClin 300 (SURPELCO) diluted 1:600, 1% BSA, and 0.15 M NaCl] for 24 h at 4 °C; 100 μL of vRAGE at various concentrations in buffer D was added to each well of the plates. Wells were washed four times and incubated for 90 min at 25 °C with 100 μL of the RAGE antibody. Following washing, wells were incubated for 90 min at 25 °C with 100 μL of the donkey anti-goat IgG-HRP antibody. Wells were washed four times and incubated with 100 μL of TMB One Solution (Promega) for 10 min. The reaction was stopped by adding 100 μL of 1 M H_2SO_4, and the absorbance was measured at 450 nm. The wells without AGE were treated in the same way to determine the background.

Surface Plasmon Resonance (SPR) Assays. The SPR assays were carried out with a BIAcore 2000 system. BSA or L-lysine was immobilized on a CM5 research grade sensor chip (GE Healthcare). Coupling was achieved with an amine coupling kit (GE Healthcare) to a density of approximately 3500 response units and 400 units, respectively, according to standard amine coupling procedures. The sensor chip was soaked in sodium phosphate (pH 7.4) containing 0.5 M DL-glyceraldehydes (Nacalai Tesque) at 37 °C for 1 week. The binding of vRAGE to this immobilized AGE fraction was examined at 25 °C with a flow rate of 20 μL/min. As the

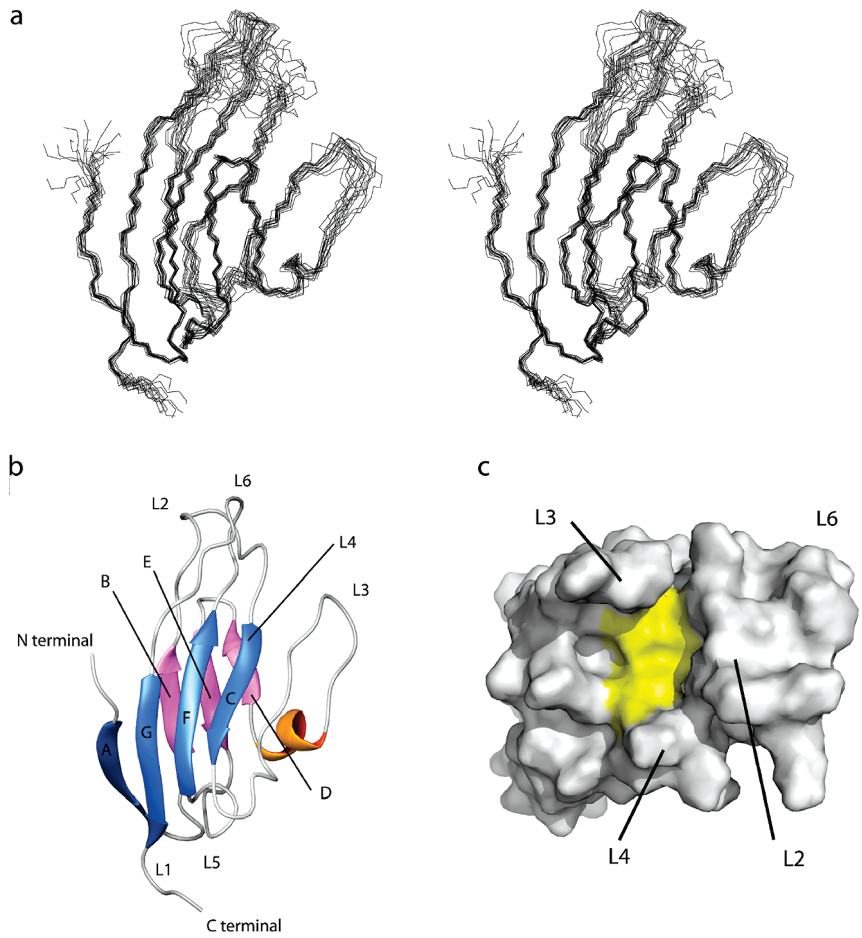

FIGURE 5: (a) Stereoview of the ensemble of 15 structures of vRAGE with the lowest energy of the target function. (b) Ribbon representations of vRAGE. The structure closest to the average of the ensemble is represented in the ribbon diagram. The α-helix is colored orange. The β-strands are colored blue (β-sheet 1) and purple (β-sheet 2) and conventionally labeled as A, B, C, D, E, F, and G. The six loops connecting these β-strands are labeled L1, L2, L3, L4, L5, and L6 starting from the N-terminal. (c) Molecular surface representation of vRAGE. The residues comprising the hydrophobic cavity, Leu49, Trp51, Leu64, Val78, and Leu84, are mapped on the molecular surface as the yellow portion.

flow buffer, 10 mM HEPES buffer (pH 7.4) containing 0.15 M NaCl, 3 mM Na-EDTA, and 0.005% (w/v) surfactant P-20 was employed. Sensor chips were regenerated when they were washed with 120 μL of 50 mM NaOH and 0.5% (w/v) sodium dodecyl sulfate (SDS).

As necessary, the data of SPR were collected by changing the duration of the association phase (T_a) ranging from 1 to 25 min while keeping the flow rate constant (10 μL/min).

To correct for refractive index change caused by nonspecific binding, the responses obtained from the control surface were subtracted from the AGE surface data. BIAevaluation version 3.0 was used to estimate affinity constants and to carry out the conventional analysis of the kinetics.

RESULTS

Expression and Characterizations of vRAGE in E. coli. Considering the results of the sequence alignment with known immunoglobulin family sequences and the secondary structure prediction, the peptide fragment of 99 amino acid residues between Ala23 and Pro121 of the native receptor, RAGE, was overexpressed and named the V-type domain (vRAGE).

Recombinant vRAGE was successfully obtained as a soluble protein. The fact that the SDS−PAGE analysis of the purified products exhibited a single band corresponding to the expected molecular mass of 11 kDa in the absence of reducing agents and there was no free thiol group detected by Ellman's analysis (*26*) confirmed the formation of the disulfide between the two cysteine residues of the peptide, Cys38 and Cys99. As shown in Figure 2, the sedimentation equilibrium analysis clearly showed that the mean molecular mass at infinite dilution is 11.8 kDa, which corresponds to the chemically expected value. Furthermore, there is no large concentration dependency detected over a wide range of concentrations up to 5.2 mg/mL (470 μM), where the NOESY measurements were carried out. This proved that the NMR sample existed in its monomer state.

To investigate the AGE binding properties of vRAGE, we carried out ELISAs and SPR assays using Lys−AGE and BSA−AGE as the ligands. As shown in Figure 3a, in the ELISAs, the absorbance of HRP, which indicates the amounts of AGE−vRAGE complexes, was increased in a concentration-dependent manner (up to 400 nM vRAGE). The affinities of vRAGE for both BSA−AGE and Lys−AGE in the nanomolar range were consistent with the affinity of RAGE determined in the case of human esRAGE obtained from COS-7 cells (*27*). In the SPR assays, the binding of vRAGE to both BSA−AGE and Lys−AGE was also observed (Figure 3b), and their K_D values were determined to be 6.2×10^{-6} and 1.9×10^{-5} M, respectively. The fact

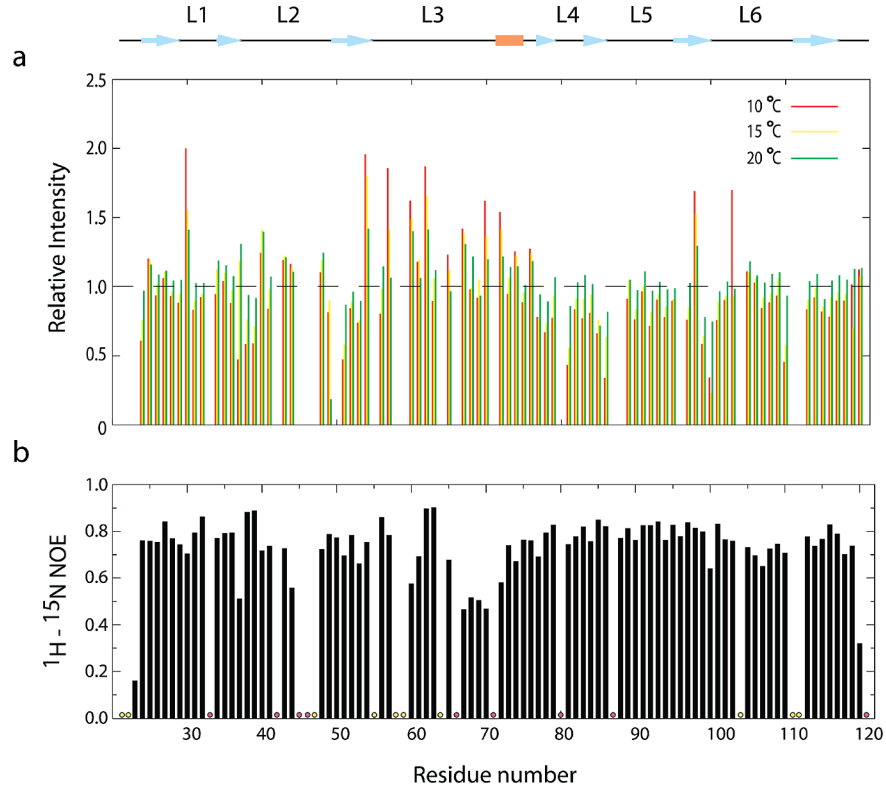

FIGURE 6: (a) Relative intensities of ^{1}H−^{15}N HSQC signals measured at 20 (green bars), 15 (yellow bars), and 10 °C (red bars) compared to those measured at 25 °C. The dashed line indicates that the value of the relative intensity is 1. The peak intensities of the cross-peaks of Gln24, Lys37, Glu50, Ala88, and Ile96 could not be analyzed due to the resonance overlap. (b) Results of ^{1}H−^{15}N steady state NOE experiments for backbone amide groups. Data for prolines and unassigned residues are represented by red circles and yellow circles, respectively. The secondary structure diagram of vRAGE is shown at the top. In the diagram, the α-helix is colored orange and β-strands and the other parts are colored blue and black, respectively.

that no rise in the response after sample injection on the blank cell was observed proved that nonspecific binding was not significant. Thus, it is confirmed that vRAGE expressed in *E. coli* retains the AGE binding activities.

Resonance Assignments in NMR Spectra. Uniformly ^{15}N- and ^{13}C-labeled vRAGE gave a well-resolved ^{1}H−^{15}N HSQC spectrum, which is shown in Figure 4, suggesting that the protein was stably folded. In the spectrum of the protein which is composed of 101 residues and contains eight prolyl residues, 95 peaks were detected. Some of them were weak due to the exchange of protons at the relatively high pH of 7.5. To complement the ambiguities with the suppression of the rapid exchange of the amide protons with bulk solvent, we measured additional ^{1}H−^{15}N HSQC spectra at lower temperatures (10, 15, and 20 °C). It made the signal intensities of some of the peaks stronger as the temperature was decreased, indicating that the amide protons providing these resonances are highly exposed to the bulk solvent. Approximately 90% of the backbone resonances and 80% of the side chain resonances were assigned and deposited in BMRB (accession number 7364). These assignments are shown in Figure 4. Although the majority is structurally homogeneous, the existence of the minor components is presumed by additional minor cross-peaks which were not assigned. These might be due to cis−trans isomerism at prolyl residues.

Structural Descriptions. Structural calculations were carried out with CNS solve 1.1 using 1032 distance restraints derived from ^{13}C-separated NOESY and ^{15}N-separated NOESY spectra, 110 pairs of backbone torsion angle restraints derived from TALOS, 42 restraints for 21 hydrogen bonds, and the restraints from one disulfide bond between Cys38 and Cys99. These experimental restraints are summarized in Table 1. Fifteen resultant structures with the lowest energy of target functions are shown in superimposition in Figure 5a. (The atomic coordinates of these structures have been deposited in the Protein Data Bank as entry 2E5E.)

Their rmsd was 0.40 Å for backbone atoms and 0.73 Å for heavy atoms in the structured regions comprised of Gln24−Lys37, Leu49−Thr55, Pro71−Gln100, and Tyr113−Val117. PROCHECK-NMR (*25*) analysis showed that 86.4 and 13.6% of the backbone angles lay in regions of Ramachandran space classified as most favored and additionally allowed, respectively. The structural statistics for the 15 structures are listed in Table. 1. It is obvious that vRAGE takes a structure similar to those of V-type domains of immunoglobulins as shown in Figure 5b with a ribbon diagram of the structure closest to the average of the ensemble. As a typical immunoglobulin fold, the structure consists of seven β-strands connected by six loops which form two β-sheets. The disulfide bond between Cys38 and Cys99 connects these sheets to form a β-sandwich structure. Secondary structure elements are labeled according to the convention of immunoglobulin as shown in Figure 5b (*28*). There are two distinct regions different from conventional immunoglobulin structures. One is an additional α-helix following L3 defined by the sequential NH_i−NH_{i+1} NOEs with strong intensities found in the peptide segment of five residues (Trp72-Asp73-Ser74-Val75-Ala76) (Figure S1 of the Supporting Information). The other is the lack of two β-strands which were found in the conventional V-type domain of immunoglobulin and named C′ and C″. There

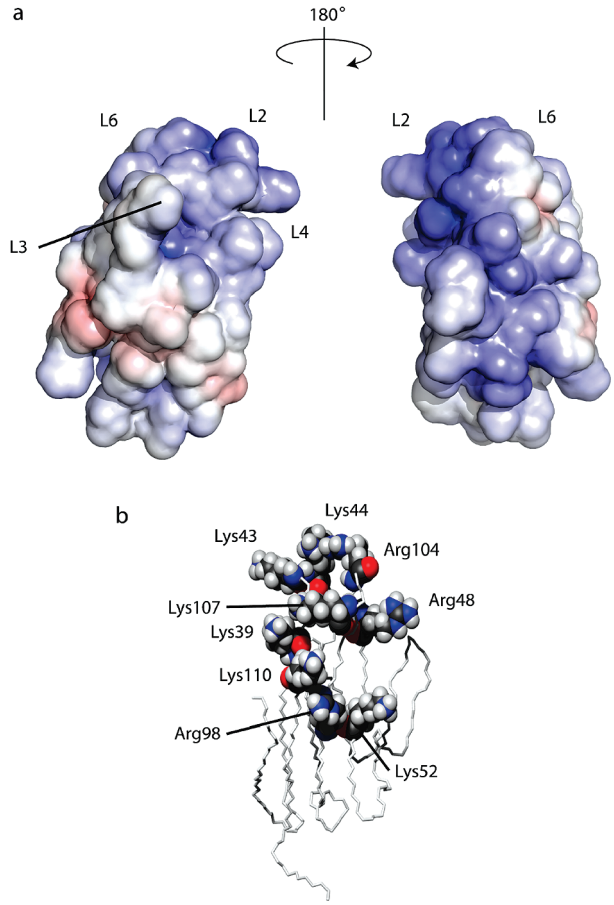

FIGURE 7: (a) Electrostatic potential distribution on the solvent accessible surface of vRAGE. Electrostatic potentials are plotted on the solvent accessible surface of vRAGE from −8 (red) to 8 *kT*/*e* (blue), where *k* is the Boltzmann constant, *T* is the temperature, and *e* is the charge of the electron. The calculation was carried out using APBS (*40*) via a PyMOL plug-in (http://www-personal.umich.edu/~mlerner/PyMOL/). (b) CPK representations of the residues substituted with Ala in the site-directed mutagenesis studies of AGE binding activities.

are extended structures in the corresponding regions of vRAGE without any defined secondary structures to form a long loop like L3.

The intensities of some peaks in the $^{1}H-^{15}N$ HSQC spectrum were gradually increased as the temperature was decreased (Figure 6a). These cross-peaks were mainly located on L3. Additionally, in the $^{1}H-^{15}N$ steady state NOE experiments for backbone amide groups, the L3 region (Thr55−Pro71) exhibited relatively low NOE values, indicating higher flexibilities (Figure 6b). These characteristic observations suggested that the L3 region is exposed to the bulk solvent and fluctuates rapidly in solution.

A large cavity and the local distribution of charged residues characterize the molecular surface as shown in Figures 5c and 7a, respectively. Leu49, Trp51, Leu64, Val78, and Leu84 form a large hydrophobic cavity around L2, L3, and L4, of which the solvent accessible surface area is −300 Å^2. The electrostatic surface potential of vRAGE analyzed by APBS revealed that the molecular surface is covered by positive charges as a whole. In particular, there is a distinguishable area where positive charges are densely localized to form a cationic center. This consists of Lys39, Lys43, Lys44, and Arg48 on the L2 loop, Lys52 on the C strand, Arg98 on the F strand, and Lys104, Arg107, and Lys110 on the L6 loop with an exceptional negative charge of Glu30 (Figure 7).

Site-Directed Mutagenesis Studies of the AGE Binding Activities of vRAGE. All mutants of vRAGE, of which each basic residue in the cationic center mentioned above was substituted with Ala, were successfully expressed in soluble fractions. They exhibited circular dichroism spectra which were almost identical to that of wild-type vRAGE, indicating that the mutagenesis did not introduce any large conformational changes into vRAGE (data not shown). This was confirmed in the case of the triply substituted mutant of vRAGE by NMR as described below.

The AGE binding activities of the each mutant were evaluated by ELISAs using Lys−AGE as the ligand. The amounts of complex formation between vRAGE and Lys−AGE at a concentration of 400 nM for each mutant are shown in Figure 8a, where the relative amount is normalized to the case of wild-type RAGE as unity. As shown in Figure 8a, drastic reductions in the level of complex formation occurred on the six mutants among them, whereas there were no large differences detected on the three remaining mutants. The former six were K43A, K44A, R48A, K52A, R98A, and R104A, and the latter three were K39A, K107A, and K110A.

Using BSA−AGE as a ligand, ELISAs were carried out on these mutants as well. Although the differences were not so distinct, the amounts of complex formation were reduced in a manner almost similar to those in the case of Lys−AGE as shown in panels a and b of Figure 8. To clarify the manner of reduction, further experiments were performed on the multiple mutants with the combination of substitution. Using the three residues, Lys43, Lys44, and Arg104, of which substitution showed the largest reduction in the case of BSA−AGE, the double mutant, K43A/R104A, and the triple mutant, K43A/K44A/R104A, were produced so their activities could be evaluated. As shown in Figure 8b, the double mutation gave a significant reduction, and it is evident that the triple mutation abolished the activity almost completely.

The binding properties of the mutants were also evaluated by the SPR assays. As shown in Figure 8c, reductions of response signals were significant for each mutant with a single substitution, K43A, K44A, or R104A, and also multiple mutants. These results of ELISAs and SPR assays indicate that the reductions in the binding ability of vRAGE mutants reflect the effect of the substitution in an additive manner.

To estimate how these multiple substitutions of cationic residues with Ala are reflected in the conformation of the vRAGE molecule, the HSQC spectrum of the triple mutant which might suffer the largest effect among all the mutants was compared with that of wild-type vRAGE (Figure S2 of the Supporting Information). The result shows that relevant chemical shift differences compared to those of wild-type vRAGE were locally detected for NH cross-peaks of the amide groups around the substituted sites. This fact clarifies that even the triple mutation did not introduce any large conformational changes into the molecular structure and thus strongly indicates that the significant reduction in activity is not caused by long-range conformational change.

We have known that vRAGE contains anionic glycan on Asn25 and Asn81 (Figure 10). Although there have been few studies of the roles of carbohydrate chains in AGE

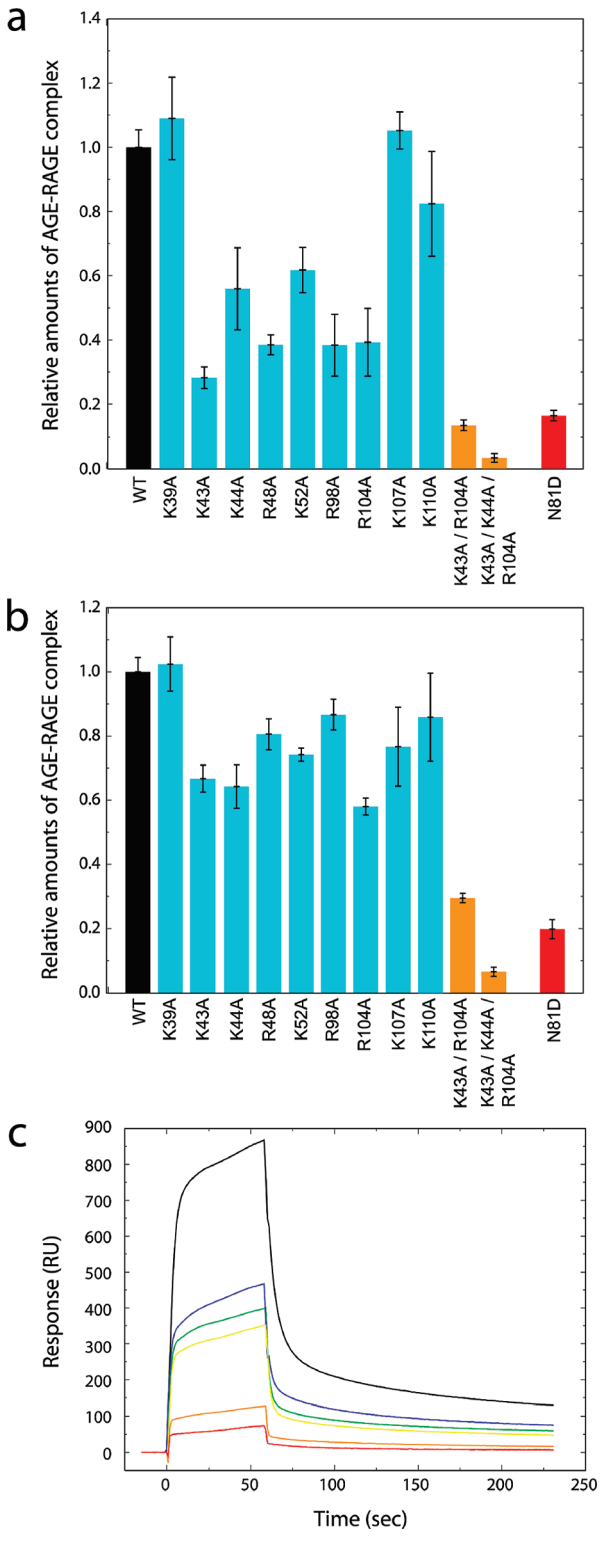

FIGURE 8: Relative amounts of Lys−AGE−RAGE (a) and BSA−AGE−RAGE (b) complexes at a protein concentration of 400 μM (WT = 1). Data for wild-type vRAGE are represented by black bars. Data for the single mutants except for N81D are represented by light blue bars. Data for the multiple mutants, K43A/R104A and K43A/K44A/R104A, are represented by orange bars. Data for the N81D mutant are represented by red bars. Bars represent standard errors (n = 3). (c) Sensorgrams derived from the binding of wild-type vRAGE and mutants to the immobilized BSA−AGE. Data for the wild type, K44A, K43A, R104A, K43A/R104A, and K43A/K44A/R104A are represented by black, blue, green, yellow, orange, and red lines, respectively. The concentrations of proteins were 1.0 μM.

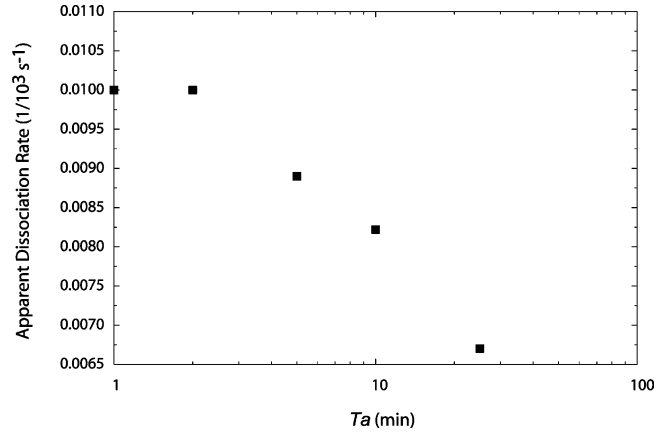

FIGURE 9: Calculated apparent dissociation constants (for the first 1 min) as a function of the length of the association period (T_a) for association of vRAGE with BSA−AGE.

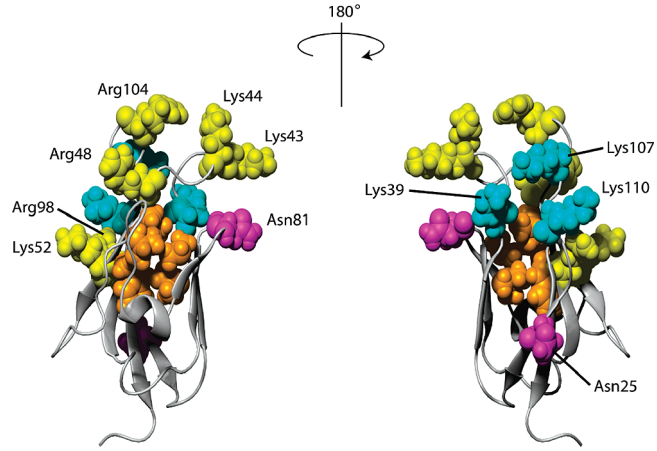

FIGURE 10: Relative arrangement between the substituted sites and the hydrophobic cavity. The residues belonging to groups 1 and 2 are colored yellow and cyan, respectively. The side chains of the residues comprising the hydrophobic cavity are colored orange. Two potential N-glycosylation sites are colored magenta.

recognition, an increase in the binding affinity with the deglycosylation at position 81 from the RAGE molecule was reported (*29*). To examine the effect of the anionic charge at position 81 on the AGE binding activity, the substitution of Asp for Asn81 was carried out, and the activity of the mutant was evaluated by using an ELISA with Lys−AGE and BSA−AGE. This single mutation was shown also to cause a significant reduction in the activity as shown in panels a and b of Figure 8. It has been shown by NMR that any long-range conformational change was not introduced by this substitution, as well (Figure S3 of the Supporting Information).

Kinetic Analysis of AGE−RAGE Binding. A kinetic analysis of the response curves of the binding of Lys−AGE to vRAGE was carried out with BIAevaluation. The analysis using the simplest model, i.e., the so-called 1:1 (Langmuir) model which is equivalent to the Langmuir isotherm for adsorption to a surface, gave values of 1.6×10^3 M^{-1} s^{-1} for the on-rate and 3.0×10^{-2} s^{-1} for the off-rate. In this case, the χ^2 value, which is the degree of closeness in the least-squares fitting, was 0.7. This indicated that this model fitted well. Interestingly, while the analysis in the case of BSA−AGE using the same model gave similar kinetic constants (1.6×10^3 M^{-1} s^{-1} for the on-rate and 1.0×10^{-2} s^{-1} for the off-rate), the χ^2 value was 1800. This value

indicates the fit with this model is rather poor. Then, the response curve was analyzed by the two-state (conformational change) model provided in the program. This is based on the assumption that the complex undergoes a conformational change after binding of the analyte on the immobilized ligand and that dissociation can occur only on the conformationally changed complex in a reversible manner. The four rate constants corresponding to k_{a1}, k_{d1}, k_{a2}, and k_{d2} in the following equation for the association−dissociation reaction were obtained.

$$A + B \underset{k_{d1}}{\overset{k_{a1}}{\rightleftharpoons}} AB^* \underset{k_{d2}}{\overset{k_{a2}}{\rightleftharpoons}} AB$$

where A and B represent BSA−AGE and vRAGE, respectively, and AB* and AB represent their encounter complex at the transition state and the stable complex, respectively. The association and dissociation constants for the first step are 2.0×10^3 M^{-1} s^{-1} and 2.2×10^{-2} s^{-1}, respectively, and those for the second step after the conformation change are 3.4×10^{-3} and 2.9×10^{-3} s^{-1}, respectively. In this case, the χ^2 value was 64. Judging from these χ^2 values, the two-state model with a conformational change is likely to fit the profile for binding of BSA−AGE to vRAGE. This implies the association−dissociation process could occur in two phases.

This hypothesis was supported by the strategy which was developed by Smith-Gill et al. as follows (*30*). First, we recorded several sensorgrams of the BSA−AGE and vRAGE system by varying the length of the association period and then analyzed each sensorgram using the 1:1 Langmuir model to estimate apparent dissociation constants for each curve. The results are plotted versus the length of the association period (T_a) in Figure 9. It is obvious that the apparent dissociation constants decrease as the T_a increases. This can be explained as Smith-Gill et al. interpreted that these changes in apparent dissociation constants depending on T_a by the change in conformation of the complex. Their antigen−antibody system included conformational flexibilities which were proven beforehand. Their explanation is that, in the beginning at short T_a values where the encounter complex is dominant, the apparent dissociation constant reflects mainly the dissociation from the encounter complex, but over time, it gradually decreases by reflecting the increase in the amount of the more stable complex. The existence of a slow conformational change to a stable complex would make the two-phase profile of the apparent dissociation constant prominent.

DISCUSSION

To carry out experiments to investigate the AGE−RAGE interaction at the molecular level, some compounds which have been well characterized to work as AGE were required. Several chemicals with low molecular weights, such as N^{ε}-carboxymethyllysine (CML) (*31*), glyceraldehyde-related pyridinium (GLAP) (*32, 33*), GA-pyridine (*34*), pentosidine (*35*), and crossline (*36*) which were isolated from reaction products between compounds containing amino groups and ones containing aldehyde groups, were found in human tissues and recognized to be compounds related to AGE. However, they did not exhibit sufficient activity to induce the intracellular signal transduction like an activation of NF-κB. So far, there has been no example in which AGE with a high affinity for RAGE was identified as an isolated compound from the products of the Maillard reaction with proteins. Under these circumstances, we chose first BSA−AGE, for which binding activities have been proven in both in vivo and in vitro systems, as a ligand to RAGE for our ELISA and SPR assays. Here, we had to keep in mind the fact not only that BSA−AGE are necessarily not only heterogeneous but also that the BSA molecule itself might have various amino groups capable of reacting with aldehydes. Furthermore, BSA−AGE is much larger than vRAGE. These facts would make the system too complicated. To confirm the results of binding assays, we repeated the same experiments with a small ligand using Lys−AGE even though it does not have in vivo activity. In both ELISAs, where BSA−AGE and Lys−AGE were used as ligands, binding of vRAGE to the immobilized ligand was observed in a concentration-dependent manner. In addition, both ligands bound to vRAGE with relatively equal affinity in SPR assays, where the K_D values of BSA−AGE and Lys−AGE were 6.2×10^{-6} and 1.9×10^{-5} M, respectively. Thus, apparently there was no essential difference detected in the binding of vRAGE with these ligands.

In the work presented here, we determined the first structure of the AGE binding domain of RAGE to be quite similar to the structures of V-type domains of immunoglobulins.

In the course of the structure determination, NMR analysis revealed the unique properties of the loop region of L3 of vRAGE. The signals from this region in $^1H-^{15}N$ HSQC and $^1H-^{15}N$ steady state NOE spectra of vRAGE were exceptionally weaker than others. In the common V-type immunoglobulin fold, two β-strands which constitute a β-sheet are found in the region corresponding to L3 but are lacking in vRAGE. The NOEs and temperature dependence of these signals indicated that this region is highly flexible. These dynamic properties should be related to the plasticity of the hydrophobic cavity which characterizes the molecular surface of vRAGE and contributes to ligand binding.

The electrostatic surface potential profile of vRAGE which was calculated by using the atomic coordinates of the resulting structure revealed that the overall surface of the molecule is positively charged. This might provide a clue for investigation of the manner of the AGE−RAGE interaction. AGE are, on the other hand, generally considered to be negatively charged because the AGE forming reaction where reducing sugars or aldehydes modify amino groups of arginine and lysine residues in proteins to produce glycated proteins adds a net negative charge on the proteins at physiological pH (*37, 38*). Thus, we assumed, as surface charge properties are frequently involved in the functional roles in ligand−receptor interactions, that charge−charge interaction should be predominantly determined by the AGE−RAGE binding system.

Each of the Lys and Arg residues located in the highly positive charged regions which were revealed in the surface potential diagram was substituted with Ala. Among eight Lys and eight Arg residues in the vRAGE molecule, there are six Lys and three Arg residues in the region. The nine total basic residues are classified into two groups by the extent of reduction of the AGE binding activity caused by the substitution. Interestingly, as shown in Figure 7b, the distribution of these residues on the resulting structure clearly

shows that they are segregated into two groups in the space corresponding to the classification of the amount of activity lost. The residues in group 1 (colored yellow in Figure 10) which exhibited large reductions surround the hydrophobic cavity. On the other hand, the residues belonging to group 2, of which substitution had little affect on activity (colored cyan in Figure 10), are located on the opposite side of the molecule with regard to the cavity.

Aiming to elucidate more information about the AGE−RAGE interaction, we tried NMR titration experiments. As Lys−AGE were titrated into the solution of ^{15}N-labeled wild-type vRAGE, a uniform decrease in the signal intensities was observed for almost all resonances in the ^{1}H−^{15}N HSQC spectra. When BSA−AGE were used, precipitation occurred immediately after the addition of the ligand. Thus, although we failed to identify the binding site by detecting the site-specific change in the NMR signal, these experiments indicated that the binding of AGE to RAGE induces the oligomerization of the protein as frequently observed for other cell surface receptors. Similar results were reported in the case of the titration experiments of the RAGE variant with S100B (*16*).

On the other hand, no apparent changes in the spectra were observed when Lys−AGE were titrated into a solution of the triple mutant. This confirmed that the triple mutant does not interact with Lys−AGE.

The introduction of one acidic residue was shown to produce a remarkable reduction in the activity as well. The AGE binding activity of the mutant in which Asn81 was substituted with an Asp residue was reduced in the ELISA experiment as shown in Figure 8a. This may be due to the repulsion of this additional negative charge from the negatively charged AGE. It has been shown that wild-type RAGE contains an anionic glycan on Asn81. Although there have been few studies of the role of carbohydrate chains in AGE recognition, an increase in the binding affinity by deglycosylation from the RAGE molecule was reported (*39*). The substitution of Asn81 with Asp could be considered as a mimic of the glycosylation of wild-type RAGE from the aspect of the addition of a negative charge. These significant effects on the activity further support the importance of the electrostatic interaction.

In addition to the fact that the charge−charge interaction is revealed to be crucial, we found another curious phenomenon. The complexes between BSA−AGE and vRAGE were hard to dissociate even with 1.0 M sodium chloride in the SPR experiment. The addition of SDS in 1.0 M sodium chloride facilitated the dissociation; e.g., 120 μL of 0.5% SDS in 1.0 M sodium chloride removed up to 80% of BSA−AGE from vRAGE. The complete dissociation was achieved by using a solution of 120 μL of 50 mM NaOH and 0.5% (w/v) SDS, which is recommended for regeneration of the surface of sensor chips in the instruction manual. On the other hand, the complexes between Lys−AGE and vRAGE were dissociated easily with the conventional condition with 1.0 M sodium chloride. The observation, where the complete disruption of the complex between BSA−AGE and vRAGE required such a forceful condition, implies there is a possibility that general AGE, which are products of the Maillard reaction with proteins, might accomplish their binding to vRAGE via not only charge−charge interactions but also some additional interactions.

Hydrophobic interaction might be the most convincing candidate for this additional interaction. The distinct hydrophobic cavity around L2, L3, and L4, which is close to the basic residues belonging to group 1 in the cationic center of vRAGE, would form a pocket that could play a role in binding BSA−AGE (Figures 5c and 7a).

The kinetic analysis of the binding of vRAGE to BSA−AGE and the time course measurements by SPR experiments, which suggest the existence of distinct phases in the interaction (Figure 9), support the involvement of the hydrophobic interaction in addition to the charge−charge interaction.

When taking the structural properties of vRAGE illustrated in Figure 10 into consideration, by analogy with the case of Smith-Gill et al. (*30*), we propose that the mechanism of the binding between BSA−AGE and RAGE occurs by these interactions. This mechanism consists of the following steps: (i) the ionic attraction between positive charges of RAGE and negative charges of AGE and (ii) the stabilization of the complex with hydrophobic interaction after conformational changes. The conformational change in the cavity might occur to alter the size of the pocket, which is rather large in the free form of vRAGE, and to fix the AGE with hydrophobic interactions in the complex.

This hypothesis could explain the fact that the basic residues belonging to group 1 exhibited a drastic reduction in the level of complex formation, but those belonging to group 2 exhibited a slight reduction as follows.

The basic residues belonging to group 1 in the cationic center and the hydrophobic pocket are in the proximity of one another, and the cavity around L3 has the dynamic property of adaptable shape. Thus, although AGE might have equal access to basic residues at the cationic center of vRAGE, only AGE which interact with the residues of group 1 are likely to move to the hydrophobic pocket with plasticity and be trapped there. On the other hand, AGE that interact with the residues of group 2, located on the opposite side of the vRAGE, cannot move to the pocket to be trapped.

Currently, the AGE−RAGE system is a focus as a key system in the development of diabetic vascular complications. Studies presented here are the first insights into the AGE−RAGE binding based on the structure of the receptor. These insights may provide important clues with respect to finding compounds to inhibit the AGE−RAGE interaction or help the rational design of therapeutic candidates for diabetic vascular complications.

ACKNOWLEDGMENT

We gratefully acknowledge T. Morikawa, K. Obata, H. Tamei, and I. Yasumatsu for their involvement in the early stage of this study. We gratefully acknowledge Dr. S. Uchiyama of the Department of Biotechnology, Graduate School of Engineering, Osaka University, for various discussions and Dr. K. Akagi of the National Institute of Biomedical Innovation (Laboratory of Cell Signal and Metabolism) for the assistance with NMR measurements. We thank S. Oka, M. Fujii, T. Maruno, and N. Fujita for their assistance.

SUPPORTING INFORMATION AVAILABLE

One figure showing a strip plot of the ^{15}N NOESY spectrum in the α-helical segment of five residues, Trp72−Ala76,

and two figures showing the overlaid $^{1}H-^{15}N$ HSQC spectra of wild-type vRAGE and the triple mutant and those of wild-type vRAGE and the N81D mutant. This material is available free of charge via the Internet at http://pubs.acs.org.

REFERENCES

1. Brownlee, M. (2001) Biochemistry and molecular cell biology of diabetic complications. *Nature 414*, 813–820.
2. Sakurai, S., Yonekura, H., Yamamoto, Y., Watanabe, T., Tanaka, N., Li, H., Rahman, A. K., Myint, K. M., Kim, C. H., and Yamamoto, H. (2003) The AGE-RAGE system and diabetic nephropathy. *J. Am. Soc. Nephrol. 14*, S259–S263.
3. Wautier, J. L., and Schmidt, A. M. (2004) Protein glycation: A firm link to endothelial cell dysfunction. *Circ. Res. 95*, 233–238.
4. Monnier, V. M., and Cerami, A. (1981) Nonenzymatic browning in vivo: Possible process for aging of long-lived proteins. *Science 211*, 491–493.
5. Li, J., and Schmidt, A. M. (1997) Characterization and functional analysis of the promoter of RAGE, the receptor for advanced glycation end products. *J. Biol. Chem. 272*, 16498–16506.
6. Neeper, M., Schmidt, A. M., Brett, J., Yan, S. D., Wang, F., Pan, Y. C., Elliston, K., Stern, D., and Shaw, A. (1992) Cloning and expression of a cell surface receptor for advanced glycosylation end products of proteins. *J. Biol. Chem. 267*, 14998–15004.
7. Schmidt, A. M., Yan, S. D., Wautier, J. L., and Stern, D. (1999) Activation of receptor for advanced glycation end products: A mechanism for chronic vascular dysfunction in diabetic vasculopathy and atherosclerosis. *Circ. Res. 84*, 489–497.
8. Yamamoto, Y., Kato, I., Doi, T., Yonekura, H., Ohashi, S., Takeuchi, M., Watanabe, T., Yamagishi, S., Sakurai, S., Takasawa, S., Okamoto, H., and Yamamoto, H. (2001) Development and prevention of advanced diabetic nephropathy in RAGE-overexpressing mice. *J. Clin. Invest. 108*, 261–268.
9. Myint, K. M., Yamamoto, Y., Doi, T., Kato, I., Harashima, A., Yonekura, H., Watanabe, T., Shinohara, H., Takeuchi, M., Tsuneyama, K., Hashimoto, N., Asano, M., Takasawa, S., Okamoto, H., and Yamamoto, H. (2006) RAGE control of diabetic nephropathy in a mouse model: Effects of RAGE gene disruption and administration of low-molecular weight heparin. *Diabetes 55*, 2510–2522.
10. Huttunen, H. J., Fages, C., and Rauvala, H. (1999) Receptor for advanced glycation end products (RAGE)-mediated neurite outgrowth and activation of NF-κB require the cytoplasmic domain of the receptor but different downstream signaling pathways. *J. Biol. Chem. 274*, 19919–19924.
11. Yan, S. D., Schmidt, A. M., Anderson, G. M., Zhang, J., Brett, J., Zou, Y. S., Pinsky, D., and Stern, D. (1994) Enhanced cellular oxidant stress by the interaction of advanced glycation end products with their receptors/binding proteins. *J. Biol. Chem. 269*, 9889–9897.
12. Tanaka, N., Yonekura, H., Yamagishi, S., Fujimori, H., Yamamoto, Y., and Yamamoto, H. (2000) The receptor for advanced glycation end products is induced by the glycation products themselves and tumor necrosis factor-α through nuclear factor-κB, and by 17β-estradiol through Sp-1 in human vascular endothelial cells. *J. Biol. Chem. 275*, 25781–25790.
13. Brett, J., Schmidt, A. M., Yan, S. D., Zou, Y. S., Weidman, E., Pinsky, D., Nowygrod, R., Neeper, M., Przysiecki, C., Shaw, A., et al. (1993) Survey of the distribution of a newly characterized receptor for advanced glycation end products in tissues. *Am. J. Pathol. 143*, 1699–1712.
14. Yonekura, H., Yamamoto, Y., Sakurai, S., Petrova, R. G., Abedin, M. J., Li, H., Yasui, K., Takeuchi, M., Makita, Z., Takasawa, S., Okamoto, H., Watanabe, T., and Yamamoto, H. (2003) Novel splice variants of the receptor for advanced glycation end-products expressed in human vascular endothelial cells and pericytes, and their putative roles in diabetes-induced vascular injury. *Biochem. J. 370*, 1097–1109.
15. Sato, T., Iwaki, M., Shimogaito, N., Wu, X., Yamagishi, S., and Takeuchi, M. (2006) TAGE (toxic AGEs) theory in diabetic complications. *Curr. Mol. Med. 6*, 351–358.
16. Dattilo, B. M., Fritz, G., Leclerc, E., Kooi, C. W., Heizmann, C. W., and Chazin, W. J. (2007) The extracellular region of the receptor for advanced glycation end products is composed of two independent structural units. *Biochemistry 46*, 6957–6970.
17. Cohn, E. J. (1943) *Proteins, Amino Acids and Peptides as Ions and Dipolar Ions*, Reinhold: New York.
18. Yamagishi, S., Yonekura, H., Yamamoto, Y., Katsuno, K., Sato, F., Mita, I., Ooka, H., Satozawa, N., Kawakami, T., Nomura, M., and Yamamoto, H. (1997) Advanced glycation end products-driven angiogenesis in vitro. Induction of the growth and tube formation of human microvascular endothelial cells through autocrine vascular endothelial growth factor. *J. Biol. Chem. 272*, 8723–8730.
19. Yamamoto, H. (2000) Mechanisms of vascular injury in diabetes: Lessons from vascular cells in culture and transgenic animals. *Biomed. Rev. 11*, 19–27.
20. Kay, L. E. (1995) Pulsed field gradient multi-dimensional NMR methods for the study of protein structure and dynamics in solution. *Prog. Biophys. Mol. Biol. 63*, 277–299.
21. Delaglio, F., Grzesiek, S., Vuister, G. W., Zhu, G., Pfeifer, J., and Bax, A. (1995) NMRPipe: A multidimensional spectral processing system based on UNIX pipes. *J. Biomol. NMR 6*, 277–293.
22. Cornilescu, G., Delaglio, F., and Bax, A. (1999) Protein backbone angle restraints from searching a database for chemical shift and sequence homology. *J. Biomol. NMR 13*, 289–302.
23. Brunger, A. T., Adams, P. D., Clore, G. M., DeLano, W. L., Gros, P., Grosse-Kunstleve, R. W., Jiang, J. S., Kuszewski, J., Nilges, M., Pannu, N. S., Read, R. J., Rice, L. M., Simonson, T., and Warren, G. L. (1998) Crystallography & NMR system: A new software suite for macromolecular structure determination. *Acta Crystallogr. 54*, 905–921.
24. Koradi, R., Billeter, M., and Wuthrich, K. (1996) MOLMOL: A program for display and analysis of macromolecular structures. *J. Mol. Graphics 14*, 51–55, 29−32.
25. Laskowski, R. A., Rullmannn, J. A., MacArthur, M. W., Kaptein, R., and Thornton, J. M. (1996) AQUA and PROCHECK-NMR: Programs for checking the quality of protein structures solved by NMR. *J. Biomol. NMR 8*, 477–486.
26. Ellman, G. L. (1959) Tissue sulfhydryl groups. *Arch. Biochem. Biophys. 82*, 70–77.
27. Yamamoto, Y., Yonekura, H., Watanabe, T., Sakurai, S., Li, H., Harashima, A., Myint, K. M., Osawa, M., Takeuchi, A., Takeuchi, M., and Yamamoto, H. (2007) Short-chain aldehyde-derived ligands for RAGE and their actions on endothelial cells. *Diabetes Res. Clin. Pract. 77* (Suppl. 1), S30–S40.
28. Bork, P., Holm, L., and Sander, C. (1994) The immunoglobulin fold. Structural classification, sequence patterns and common core. *J. Mol. Biol. 242*, 309–320.
29. Srikrishna, G., Huttunen, H. J., Johansson, L., Weigle, B., Yamaguchi, Y., Rauvala, H., and Freeze, H. H. (2002) N-Glycans on the receptor for advanced glycation end products influence amphoterin binding and neurite outgrowth. *J. Neurochem. 80*, 998–1008.
30. Lipschultz, C. A., Li, Y., and Smith-Gill, S. (2000) Experimental design for analysis of complex kinetics using surface plasmon resonance. *Methods 20*, 310–318.
31. Ahmed, M. U., Thorpe, S. R., and Baynes, J. W. (1986) Identification of Nε-carboxymethyllysine as a degradation product of fructoselysine in glycated protein. *J. Biol. Chem. 261*, 4889–4894.
32. Usui, T., and Hayase, F. (2003) Isolation and identification of the 3 hydroxy-5-hydroxymethyl-pyridinium compound as a novel advanced glycation end product on glyceraldehyde-related Maillard reaction. *Biosci., Biotechnol., Biochem. 67*, 930–932.
33. Usui, T., Shizuuchi, S., Watanabe, H., and Hayase, F. (2004) Cytotoxicity and oxidative stress induced by the glyceraldehyde-related Maillard reaction products for HL-60 cells. *Biosci., Biotechnol., Biochem. 68*, 333–340.
34. Nagai, R., Hayashi, C. M., Xia, L., Takeya, M., and Horiuchi, S. (2002) Identification in human atherosclerotic lesions of GA-pyridine, a novel structure derived from glycolaldehyde-modified proteins. *J. Biol. Chem. 277*, 48905–48912.
35. Sell, D. R., and Monnier, V. M. (1989) Structure elucidation of a senescence cross-link from human extracellular matrix. Implication of pentoses in the aging process. *J. Biol. Chem. 264*, 21597–21602.
36. Obayashi, H., Nakano, K., Shigeta, H., Yamaguchi, M., Yoshimori, K., Fukui, M., Fujii, M., Kitagawa, Y., Nakamura, N., Nakamura, K., Nakazawa, Y., Ienaga, K., Ohta, M., Nishimura, M., Fukui, I., and Kondo, M. (1996) Formation of crossline as a fluorescent advanced glycation end product in vitro and in vivo. *Biochem. Biophys. Res. Commun. 226*, 37–41.
37. Westwood, M. E., and Thornalley, P. J. (1995) Molecular characteristics of methylglyoxal-modified bovine and human serum albumins. Comparison with glucose-derived advanced glycation endproduct-modified serum albumins. *J. Protein Chem. 14*, 359–372.

38. Nagai, R., Matsumoto, K., Ling, X., Suzuki, H., Araki, T., and Horiuchi, S. (2000) Glycolaldehyde, a reactive intermediate for advanced glycation end products, plays an important role in the generation of an active ligand for the macrophage scavenger receptor. *Diabetes 49*, 1714–1723.
39. Osawa, M., Yamamoto, Y., Munesue, S., Murakami, N., Sakurai, S., Watanabe, T., Yonekura, H., Uchigata, Y., Iwamoto, Y., and Yamamoto, H. (2007) De-N-glycosylation or G82S mutation of RAGE sensitizes its interaction with advanced glycation endproducts. *Biochim. Biophys. Acta 1770*, 1468–1474.
40. Baker, N. A., Sept, D., Joseph, S., Holst, M. J., and McCammon, J. A. (2001) Electrostatics of nanosystems: Application to microtubules and the ribosome. *Proc. Natl. Acad. Sci. U.S.A. 98*, 10037–10041.

BI800910V